Solar Energy Materials & Solar Cells 120 (2014) 724–727

Contents lists available at ScienceDirect

Solar Energy Materials & Solar Cells

journal homepage: www.elsevier.com/locate/solmat

Organic solar cells comprising multiple-device stacked structures exhibiting complementary absorption behavior

Wei-Ting Lin [a], Yen-Tseng Lin [b], Chu-Hsien Chou [a], Fang-Chung Chen [a,*], Chain-Shu Hsu [c]

[a] Department of Photonics, National Chiao Tung University, Hsinchu 30010, Taiwan
[b] Institute of Lighting and Energy Photonics, National Chiao Tung University, Tainan 71150, Taiwan
[c] Department of Applied Chemistry, National Chiao Tung University, Hsinchu 30010, Taiwan

ARTICLE INFO

Available online 28 August 2013

Keywords:
Organic
Photovoltaic
Multi-junction
Absorption

ABSTRACT

We developed organic solar cells based on multiple-device stacked structures featuring complementary absorption behavior. The first, semitransparent (ST) subcell featured an inverted structure; its anode comprised a MoO_3/Ag bilayer. This structure provided a transmittance of greater than 35% in the visible region. The second subcell, featuring a low-band-gap small molecule in its photoactive layer, was stacked onto the ST device; the two subcells could be connected either in series or in parallel. Because the two subcells exhibited complementary absorption behavior, their stacked structure connected in parallel displayed a power conversion efficiency of 4.37%, greater than those of the isolated subcells.

1. Introduction

Organic photovoltaic devices (OPVs) are promising candidates for use in next-generation solar cells because of their attractive properties of inexpensive fabrication, light weight, and mechanical flexibility [1–6]. The presence of bulk heterojunctions between the electron donors and acceptors in photoactive thin films can greatly improve device efficiency [1–6]. To date, the power conversion efficiency (PCE) of OPVs has reached approximately 10% in single-junction devices [1]. Increasing photon absorption is one of the key issues that must be overcome if we are to further improve PCEs. The low mobility of organic materials, however, restricts the use of thicker photoactive layers for the harvesting of greater number of photons. Moreover, the narrow absorption ranges of single materials limit the range of the solar spectrum available for absorption. One plausible method toward solving these problems is to produce tandem cells [7–11]. Nevertheless, because multi-junction devices have relatively complicated structures, the need for sophisticated fabrication procedures generally decreases the device fabrication yield.

In 2006, Shrotriya et al. proposed an alternative approach for constructing multi-junction devices: they superimposed one semi-transparent (ST) cell onto another conventional one [12]. After connecting the two subcells, either in series or in parallel, the PCE could be doubled relative to the efficiency of the corresponding single-junction device. Nevertheless, most reported stacked cells of this type have adopted the same photoactive materials in the two subcells [12–14]; as a result, multiple-device stacked structures exhibiting complementary absorptions are rare [15]. In this present study, we used two different organic materials, with complementary absorption spectra, as the photoactive layers in the two subcells. The first, ST subcell adopted an inverted structure; its ST anode comprised a MoO_3/Ag bilayer. The second subcell featured a low-band-gap (LBG) small molecule (SM) in its photoactive layer; it was stacked onto the ST device such that the two subcells were connected either in series or in parallel. Because the absorption behavior of the two subcells was complementary, the stacked device exhibited improved PCE relative to that of the single-cell device.

2. Experimental

The conjugated polymer and fullerene derivative used in this study were regioregular poly(3-hexylthiophene) (P3HT) and 1-(3-methoxycarbonyl)propyl-1-phenyl[6,6]methanofullerene (PCBM), respectively. The LBG SM used in the back subcell was 2,5-di(2-ethylhexyl)-3,6-bis-(5″-*n*-hexyl-[2,2′,5′,2″]terthiophen-5-yl)-pyrrolo[3,4-*c*]pyrrole-1,4-dione (SMDPPEH) [16]. Fig. 1(a) displays the chemical structures of these materials as well as the device structure. Fig. 1(b) presents the absorption spectra of the P3HT:PCBM and SMDPPEH:PCBM thin films. The two blends cover the solar spectrum over the range from 350 to 800 nm in a complementary manner. To begin the fabrication of the ST device, a solution of Cs_2CO_3 in 2-ethoxyethanol was spin-coated onto an indium tin oxide (ITO)-coated substrate and then the substrate was baked at 140 °C for 20 min. Next, a solution of the P3HT/PCBM blend in 1,2-dicholorobenzene was coated onto the substrate.

* Corresponding author. Tel.: +886 3 5131484; fax: +886 3 5735601.
E-mail address: fcchen@mail.nctu.edu.tw (F.-C. Chen).

0927-0248/$ - see front matter © 2013 Elsevier B.V. All rights reserved.
http://dx.doi.org/10.1016/j.solmat.2013.07.043

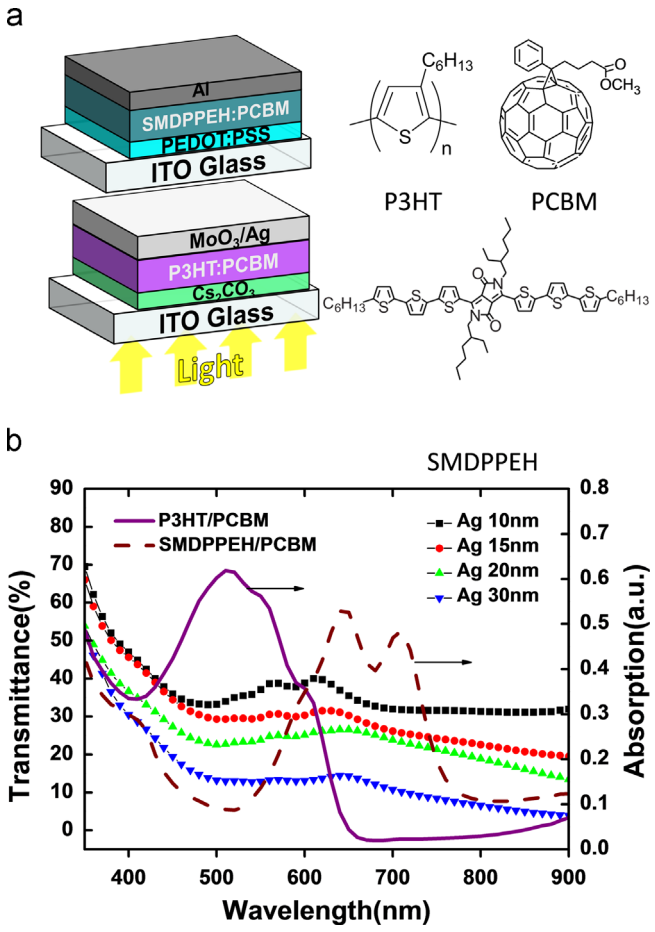

Fig. 1. (a) Chemical structures of P3HT, PCBM, and SMDPPEH. (b) Absorption spectra of films of P3HT:PCBM (1:1, w/w) and SMDPPEH:PCBM (1:1, w/w).

After solvent annealing [17,18], the sample was further thermally annealed at 110 °C for 15 min. Finally, MoO_3 (3.5 nm) and Ag (10–100 nm) were deposited to form the top electrodes; the Ag layer was chosen because of its long skin depth and high electrical conductivity [13]. Fabrication of the SM device began with spin-coating of poly(3,4-ethylenedioxythiophene):polystyrenesulfonate (PEDOT:PSS) onto an ITO-coated substrate and then baking the resulting film at 120 °C for 1 h. Next, a solution of the SMDPPEH:PCBM blend in chlorobenzene was coated on top of the PEDOT:PSS layer. Finally, Al (100 nm) was thermally evaporated to serve as the cathode. The photocurrent density–voltage (*J*–*V*) curves under illumination were recorded using a Keithley 2400 measurement system. The light source was a Thermal Oriel solar simulator, the illumination intensity of which was calibrated using a Si photodiode detector equipped with a KG-5 filter (Hamamatsu) [19].

3. Results and discussion

Fig. 2(a) displays the *J*–*V* curves of ST devices fabricated with various Ag thicknesses. Although the device fabricated with a 10-nm-thick Ag anode had the highest transmittance [Fig. 1(b)], it exhibited relatively poor performance, with a PCE of 2.36%. When we increased the thickness of the Ag layer to 15 nm, the transmittance in the visible region was greater than 35% [Fig. 1(b)]; this ST device exhibited an open-circuit voltage (V_{oc}) of 0.57 V, a short-circuit current (J_{sc}) of 8.53 mA cm^{-2}, and a fill factor (FF) of 0.61, leading to a PCE of 2.97%. In general, the device efficiency improved upon increasing the thickness of the Ag layer, suggesting

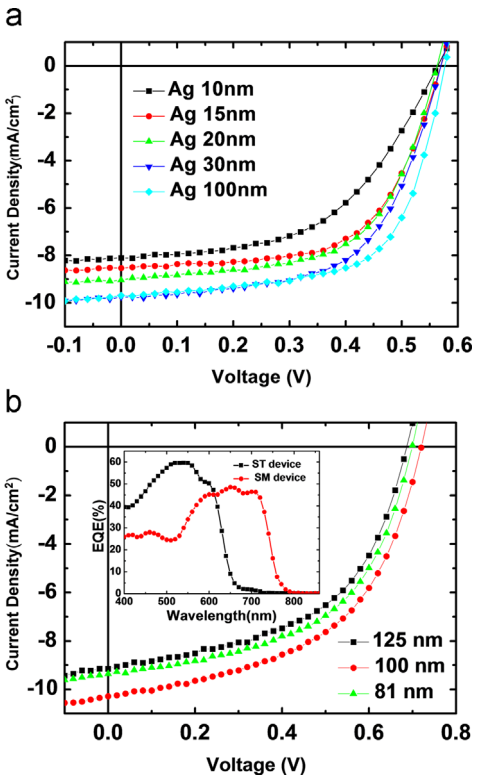

Fig. 2. (a) *J*–*V* characteristics of ST devices prepared with Ag layers of various thicknesses. (b) *J*–*V* curves of SM devices prepared with photoactive layers of various thicknesses. Inset: EQE spectra of the two subcells in the stacked structure. Structures of the ST and SM devices: ITO/PEDOT:PSS/P3HT:PCBM (220 nm)/MoO_3 (3.5 nm)/Ag and ITO/PEDOT:PSS/SMDPPEH:PCBM (100 nm)/Al, respectively.

Table 1
Photovoltaic parameters of OPVs featuring Ag anodes of various thicknesses.

Ag thickness (nm)	V_{oc} (V)	J_{sc} (mA cm^{-2})	**FF**	**PCE** (%)
10	0.56	8.10	0.52	2.36
15	0.57	8.53	0.61	2.97
20	0.57	9.03	0.60	3.03
30	0.57	9.74	0.59	3.29
100	0.57	9.70	0.65	3.57

that the sheet resistance of the Ag anode limited the device performance. Although the highest device efficiency (3.29%) was obtained when the thickness of the Ag layer was 30 nm, the overall transmittance in the visible wavelength range was only approximately 10% [Fig. 1(b)], making this device unsuitable for use in stacked structures. Table 1 summarizes the parameters of the devices featuring Ag anodes of various thicknesses.

Fig. 2(b) presents the *J*–*V* characteristics of the SM devices obtained under the illumination with simulated solar irradiation. For the optimized device, in which the thickness of the photoactive layer was 100 nm, the values of V_{oc}, J_{sc}, and FF were 0.72 V, 10.28 mA cm^{-2}, and 0.52, respectively, yielding a PCE of 3.83%. The inset to Fig. 2(b) displays the incident photon-to-electron conversion efficiencies (IPCEs) of both the ST and SM devices. The major wavelength response ranges of the ST and SM devices were 450–600 and 600–750 nm, respectively, confirming the complementary manner of photoabsorption of these two different devices.

We constructed multiple-device stacked structures by stacking the SM device onto the inverted ST device (Fig. 1); the back SM device absorbed solar irradiation that had passed through the ST device. We tested the performance of the two subcells connected either in parallel or in series. Fig. 3(a) displays the *J*–*V* curves of the

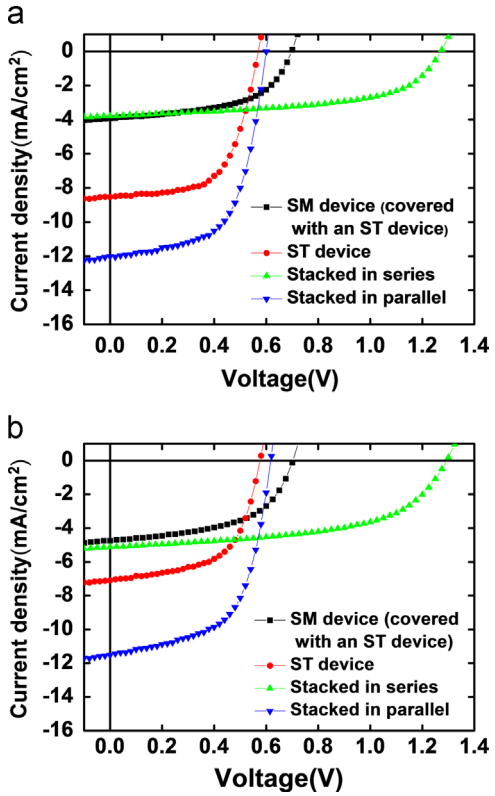

Fig. 3. *J–V* curves of the front ST subcell, the back SM subcell, and the stacked structures connected either in series or in parallel under illumination (simulated AM1.5G). Thickness of the photoactive layer of the front ST subcell: (a) 220 and (b) 100 nm.

individual subcells and of the stacked device structure. Because a portion of the photons was absorbed and/or blocked by the front ST subcell, the back SM cell exhibited a lower photocurrent (i.e., 3.91 mA cm^{-2}) than that of the device measured before connection with the ST device. The FF of the back SM alone was increased to 0.54, but the value of V_{oc} decreased slightly to 0.70 V, resulting in a PCE of 1.49%. When we connected the subcells in series, the value of V_{oc} of the whole stacked device was 1.26 V, very close to the sum of the photovoltages of the two isolated subcells (0.57 V for the ST device and 0.70 V for the SM device). Because the current in the same loop should be identical according to Kirchhoff's law, a low value of J_{sc} of 3.78 mA cm^{-2} was obtained, limited by the back subcell. Therefore, the PCE (only 2.70%) was even lower than that of the ST device measured individually under conditions of 1 sun. On the other hand, when we connected the subcells in parallel, the photocurrent increased significantly to 12.01 mA cm^{-2}; the values of V_{oc} and FF were 0.60 V and 0.60, respectively, resulting in an improved PCE of 4.37%. This value is very close to the sum of the PCEs of the individual subcells in the device (2.97% for the ST device and 1.49% for the SM device), indicating that no apparent energy loss occurred when the stacked structure was connected in parallel. Furthermore, the PCE was higher than that of either of the isolated subcells measured individually under illumination (i.e., 2.97% for the ST device and 3.83% for the SM device). Our results suggest that stacking structures is an effective approach toward assembling multiple devices containing complementary absorption behavior. Table 2 summarizes the parameters of the various stacked structures.

The thickness of the photoactive layer in the back SM subcell barely affected the performance of the stacked structure. Nevertheless, the effect of the thickness of the front subcell was significant. For example, Fig. 3(b) displays the device performance

Table 2
Photovoltaic parameters of individual subcells and stacked structures when the thickness of the P3HT:PCBM layer was 220 nm.

Device condition	V_{oc} (V)	J_{sc} (mA cm^{-2})	FF	PCE (%)
SM device under standard conditions[a]	0.72	10.28	0.52	3.83
Transparent device under standard conditions[a]	0.57	8.53	0.61	2.97
SM device in stacked structure	0.70	3.91	0.54	1.49
Transparent device in stacked structure	0.57	8.53	0.61	2.97
Stacked structure connected in series	1.26	3.78	0.57	2.70
Stacked structure connected in parallel	0.60	12.01	0.60	4.37

[a] The device was not connected to another subcell; it was measured individually.

Table 3
Photovoltaic parameters of individual subcells and stacked structures when the thickness of the P3HT:PCBM layer was 100 nm.

Device condition	V_{oc} (V)	J_{sc} (mA cm^{-2})	FF	PCE (%)
SM device under standard conditions[a]	0.72	10.28	0.52	3.83
Transparent device under standard conditions[a]	0.57	7.10	0.59	2.37
SM device in stacked structure	0.70	4.75	0.54	1.78
Transparent device in stacked structure	0.57	7.10	0.59	2.37
Stacked structure connected in series	1.27	5.12	0.56	3.64
Stacked structure connected in parallel	0.61	11.52	0.60	4.18

[a] The device was not connected to another subcell; it was measured individually.

of the stacked structure when we decreased the thickness of the P3HT:PCBM layer in the front subcell to 100 nm. First, the value of J_{sc} of the front ST device decreased to 7.10 mA cm^{-2}, presumably due to the lower degree of photon absorption; accordingly, the PCE decreased to 2.73%. Furthermore, because more photons passed through the ST cell, the value of J_{sc} of the individual SM device in the stacked device increased to 4.75 mA cm^{-2}, resulting in a higher PCE (1.78%). Because of the increased value of J_{sc} of the current-limiting subcell (i.e., the back SM subcell) for the stacked structure connected in series, the overall PCE improved to 3.64%. Notably, the stacked structure connected in parallel exhibited even better performance, with V_{oc}, J_{sc}, and FF values of 0.61 V, 11.52 mA cm^{-2}, and 0.62, respectively; its PCE was 4.18%. This value is also almost identical to the sum of the PCEs of the individual subcells (2.37% for the ST device and 1.78% for the SM device). These results reveal that, unlike the situation when the subcells were connected in series, the efficiency of the subcells connected in parallel was not limited by current matching; the subcells could still function individually when they were connected in parallel, leading to higher PCEs [14]. Table 3 summarizes the parameters of the stacked structures in which the thickness of the P3HT:PCBM layer was 100 nm.

To further support the beneficial effect of the complementary absorption behavior, we further built stacked structures containing the same photoactive materials in the two subcells. Note, however, that the device performance of the SM subcell made with the inverted structure was rather poor, presumably due to the poor film quality on the Cs_2CO_3 surfaces and/or the inferior metal/polymer contact at the cathode. We, therefore, only used P3HT:PCBM blends for device fabrication. Fig. 4 displays the device performance of the stacked structure, in which both photoactive layers were P3HT:PCBM. The back cell exhibited a typical PCE of 3.87% (V_{oc}=0.59; J_{sc}=10.38 mA cm^{-2}; FF=0.63) under 100 mW cm^{-2} illumination (AM1.5G) [18]. When the device was stacked with the front cell, the PCE decreased significantly to

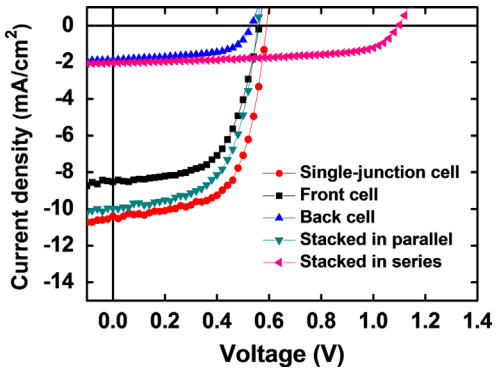

Fig. 4. *J–V* curves of the stacked structures connected either in series or in parallel under illumination (simulated AM1.5G). The photoactive layer of both subcells was P3HT:PCBM.

0.59% (V_{oc}=0.53; J_{sc}=1.83 mA cm^{-2}; FF=0.61). Again, it was due to the fact that a portion of the light was absorbed and/or blocked by the front subcell. When the subcells were connected in series, the photocurrent was only 2.03 mA cm^{-2}; the values of V_{oc} and FF were 1.09 V and 0.59, respectively, resulting in a low PCE of 1.31%. The PCE, however, became higher (3.29%) when the two subcells were connected in parallel. The values of V_{oc}, J_{sc} and FF were 0.55 V, 9.96 mA cm^{-2} and 0.60, respectively. Although a better performance was obtained compared with the efficiency of each subcell, the PCE was still lower than that (3.87%) of a typical standard single-junction cell. The results were consistent with our previous observation [14]. In short, the data presented in Fig. 4 suggests that complementary light absorption of the active layers is indeed essential for achieving even higher device performance.

4. Conclusion

Stacking multiple solar cells is a promising approach for achieving high efficiencies by reducing absorption and thermalization loss [20,21]. For double-junction solar cells based on inorganic materials, such as III–V semiconductors, there are generally two methods for combining the cells: one is to physically separate them and to use multiple contacts and the other is to integrate the subcells with tunnel junctions joining them in series [21]. For OPVs, the most common approach is to connect two subcells directly in series, which is similar to the second method. Multiple OPVs connected with the first method using a physical separated structure are still seldom reported. In this work, we have developed organic solar cells based on multiple-device stacked structures exhibiting complementary absorption behavior. We stacked an inverted ST subcell with a second subcell featuring a LBG SM; we examined the performance of the two subcells connected either in series or in parallel. Because the two subcells exhibited complementary absorption behavior, their stacked device connected in parallel provided an improved PCE. Notably, the device efficiency remained limited by certain factors; for example, when we connected the subcells in parallel, the values of V_{oc} were still relatively low. Further improvements, such as tailoring the energy-level structure to increase the photovoltage, will be performed in the future.

Acknowledgments

We thank the National Science Council of Taiwan (Grant nos. NSC 102-3113-P-009-004 and NSC 101-2628-E-009-008-MY3) and the Ministry of Education of Taiwan (through the ATU program) for financial support.

References

[1] G. Li, R. Zhu, Y. Yang, Polymer solar cells, Nature Photonics 6 (2012) 153–161.
[2] J. Zhu, X. Zhu, R. Hoekstra, L. Li, F. Xiu, M. Xue, B. Zeng, K.L. Wang, Metallic nanomesh electrodes with controllable optical properties for organic solar cells, Applied Physics Letters 100 (2012) 143109-1–143109-4.
[3] J.L. Wu, F.C. Chen, M.K. Chuang, K.S. Tan, Near-infrared laser-driven polymer photovoltaic devices and their biomedical applications, Energy and Environmental Science 4 (2011) 3374–3378.
[4] H.L. Yip, A.K.Y. Jen, Recent advances in solution-processed interfacial materials for efficient and stable polymer solar cells, Energy and Environmental Science 5 (2012) 5994–6011.
[5] J.L. Wu, F.C. Chen, Y.S. Hsiao, F.C. Chien, P. Chen, C.H. Kuo, M.H. Huang, C.S. Hsu, Surface plasmonic effects of metallic nanoparticles on the performance of polymer bulk heterojunction solar cells, ACS Nano 5 (2011) 959–967.
[6] X. Guo, C. Chi, M. Zhang, L. Huo, Y. Huang, J. Hou, Y. Li, High efficiency polymer solar cells based on poly(3-hexylthiophene)/indene-C_{70} bisadduct with solvent additive, Energy and Environmental Science 5 (2012) 7943–7949.
[7] J.Y. Kim, K. Lee, N.E. Coates, D. Moses, T.Q. Nguyen, M. Dante, A.J. Heeger, Efficient tandem polymer solar cells fabricated by all-solution processing, Science 317 (2007) 222–225.
[8] L. Dou, J. You, J. Yang, C.C. Chen, Y. He, S. Murase, T. Moriarty, K. Emery, G. Li, Y. Yang, Tandem polymer solar cells featuring a spectrally matched low-bandgap polymer, Nature Photonics 6 (2012) 180–185.
[9] S. Sista, Z. Hong, L.M. Chen, Y. Yang, Tandem polymer photovoltaic cells—current status, challenges and future outlook, Energy and Environmental Science 4 (2011) 1606–1620.
[10] V.C. Tung, J. Kim, L.J. Cote, J. Huang, Sticky interconnect for solution-processed tandem solar cells, Journal of the American Chemical Society 133 (2011) 9262–9265.
[11] F.C. Chen, C.H. Lin, Construction and characteristics of tandem organic solar cells featuring small molecule-based films on polymer-based subcells, Journal of Physics D: Applied Physics 43 (2010) 025104-1–025104-8.
[12] V. Shrotriya, E.H.E. Wu, G. Li, Y. Yao, Y. Yang, Efficient light harvesting in multiple-device stacked structure for polymer solar cells, Applied Physics Letters 88 (2006) 064104-1–064104-3.
[13] R.F. Bailey-Salzman, B.P. Rand, S.R. Forrest, Semitransparent organic photovoltaic cells, Applied Physics Letters 88 (2006) 233502-1–233502-3.
[14] W.C. Chen, S.C. Chien, F.C. Chen, C.S. Hsu, Stacked structures for assembling multiple organic photovoltaic devices, Applied Physics Express 5 (2012) 072301-1–072301-3.
[15] Z. Tang, Z. George, Z. Ma, J. Bergqvist, K. Tvingstedt, K. Vandewal, E. Wang, L.M. Andersson, M.R. Andersson, F. Zhang, O. Inganäs, Semi-transparent tandem organic solar cells with 90% internal quantum efficiency, Advanced Energy Materials 2 (2012) 1467–1476.
[16] A. Tamayo, T. Kent, M. Tantitiwat, M.A. Dante, J. Rogers, T.Q. Nguyen, Influence of alkyl substituents and thermal annealing on the film morphology and performance of solution processed, diketopyrrolopyrrole-based bulk heterojunction solar cells, Energy and Environmental Science 2 (2009) 1180–1186.
[17] G. Li, Y. Yao, H. Yang, V. Shrotriya, G. Yang, Y. Yang, Solvent annealing effect in polymer solar cells based on poly(3-hexylthiophene) and methanofullerenes, Advanced Functional Materials 17 (2007) 1636–1644.
[18] F.C. Chen, C.J. Ko, J.L. Wu, W.C. Chen, Morphological study of P3HT:PCBM blend films prepared through solvent annealing for solar cell applications, Solar Energy Materials and Solar Cells 94 (2010) 2426–2430.
[19] V. Shrotriya, G. Li, Y. Yao, T. Moriarty, K. Emery, Y. Yang, Accurate measurement and characterization of organic solar cells, Advanced Functional Materials 16 (2006) 2016–2023.
[20] R.R. Lunt, T.P. Osedach, P.R. Broen, J.A. Rowehl, B. Bulović, Practical roadmap and limits to nanostructured photovoltaics, Advanced Materials 23 (2011) 5712–5727.
[21] G.F. Brown, J. Wu, Third generation photovoltaics,, Laser and Photonics Reviews 3 (2009) 394–405.